sustainability

MDPI

Article

Black Crust from Historic Buildings as a Natural Indicator of Air Pollution: A Case Study of the Lipowiec Castle, Babice, Southern Poland

Mariola Marszałek *, Krzysztof Dudek and Adam Gaweł

Faculty of Geology, Geophysics and Environmental Protection, AGH University of Krakow, Al. Mickiewicza 30, 30-059 Kraków, Poland; kadudek@agh.edu.pl (K.D.); agawel@agh.edu.pl (A.G.)
* Correspondence: mmarszal@agh.edu.pl

Abstract: The study is focused on the analysis of black crust and soiling on the building materials of the medieval Lipowiec Castle in southern Poland. The castle was constructed using local, partly dolomitic limestones and dolomites, supplemented with other limestones and bricks, during 20th-century renovations of the castle ruins. The crust and soiling components, secondary mineral phases, and particulate matter of anthropogenic origin were analysed using Raman micro-spectroscopy (RS) and scanning electron microscopy coupled with energy-dispersive spectrometry (SEM-EDS). The crust, mostly composed of gypsum and other sulphate phases, was found to contain carbonaceous matter, spherical Si-Al glass particles, and iron oxides, with admixtures of other elements, including heavy metals, as well as irregularly shaped particles containing various metals. These components reflect the air pollution in the region, related to the combustion of solid fuels in both industrial power plants and local domestic furnaces, Zn-Pb ore mining (operational until 2021), and smelting in the neighbouring industrial centre. Despite its location in a rural area, the castle has been exposed to pollution for an extended period due to its proximity to large industrial centres. Therefore, the crust analysed may serve as an environmental indicator of the nature of the air pollution in the region.

Keywords: heritage buildings; dolomitic limestone; black crust; carbonaceous particles; air pollution

Citation: Marszałek, M.; Dudek, K.; Gaweł, A. Black Crust from Historic Buildings as a Natural Indicator of Air Pollution: A Case Study of the Lipowiec Castle, Babice, Southern Poland. *Sustainability* **2024**, *16*, 3816. https://doi.org/10.3390/su16093816

Academic Editor: Jesus Martinez-Frias

Received: 23 March 2024
Revised: 14 April 2024
Accepted: 20 April 2024
Published: 1 May 2024

1. Introduction

Stones used for the construction of external elements of historic castles and other heritage buildings are susceptible to atmospheric weathering [1]. Concurrently, industrial development in recent centuries has brought about, among other consequences, substantial deterioration in air quality, affecting not only urban areas but also rural environments. The combustion of coal and other fossil fuels, vehicular traffic, and various other industrial emissions result in atmospheric pollution from sulphur dioxide (SO_2), particulate matter (PM), and numerous other gaseous (e.g., NO_x, CO_2, H_2S, and HCl) and dusty components [2–4]. As a result, stone surfaces exposed over long periods gradually darken due to the accumulation of pollutants, particularly carbonaceous particles [5–9]. Consequently, these surfaces become coated with thin black layers and/or so-called soiling [10]. These black layers, in turn, accumulate more air pollutants and may accelerate the physicochemical deterioration of historic stones [11–17]. Black crust, appearing mainly in sites protected from direct rainfall or water runoff in urban environments, compromises the durability and aesthetic appeal of historic buildings and monuments. The crust forms a reactive surface on which other precipitates may form. This is because carbonaceous particles and metallic compounds in the particulate matter can act as active catalysts for the transformation of the substrate (e.g., calcium carbonate) to gypsum. Black crust is commonly defined as a deteriorated surface layer of hard and fragile stone material, varying in thickness [4,18–22]. Black crust, whether strongly or weakly attached to the background material, may also freely detach from the stone, especially in cases where the latter is significantly altered.

Previous studies have revealed that black crust often consists of a gypsum ($CaSO_4 \cdot 2H_2O$) matrix with atmospheric dust particles (carbonaceous, metallic, mineral, soot, ash, etc.) trapped inside, which are responsible for its dark colouration [5,8,23]. The gypsum layer, produced by the reaction of calcite from the stone or mortar with atmospheric SO_2, often exhibits high porosity, facilitating the accumulation of not only dust particles but also organic matter (e.g., microbial biomass and its metabolic products) [24,25]. Microorganisms may produce various organic acids, dissolving carbonate and even silicate rock components, and forming water-soluble salts or complexes [25–27]. Microbial cells colonising a stone surface intensify the degrading effects of pollution. The impacts of biodegradation may resemble those of physical weathering, e.g., surface roughening, the formation of small fissures, and colour changes [25]. Under such conditions, it may be difficult to distinguish non-biological stone degradation from that associated with microbiological growth. Therefore, the identification of various particles deposited on stone surfaces is crucial for analysing the causes and nature of stone deterioration [17].

Last year's studies on black crust focused on salt crystallisation and organic matter, as well as carbon and metallic (Fe, Zn, Pb, Cd, As, etc.) particle deposition [15,16,25,28–32]. Black crust and soiling may yield significant information about air quality, making them important for both the environment and human health [17,33]. Heritage building studies conducted continuously or repeatedly, over long periods of time, may yield data on variations or tendencies in air pollution, of key importance for pollution control and sustainable regional development [34,35].

In this study, Raman micro-spectroscopy (RS) and scanning electron microscopy coupled with energy-dispersive X-ray spectroscopy (SEM-EDS) were used for the analysis of soiling and black crust sampled from the ruins of Lipowiec Castle, situated in a rural area in southern Poland. The soiling and crust formed as thin, outer layers on the substrata of Triassic and Jurassic carbonate rocks (limestones and dolomites) and bricks. The study focused on mineral analysis of the crust samples, including the identification of particulate matter of anthropogenic origin, initially deposited on the surface and subsequently trapped in the growing black crust or soiling. Based on the crust components identified, possible sources of pollution were discussed. Finally, the analyses aimed to present the characteristics of the black crust from a historic building situated in the countryside. New data on the black crust developed on historic stones in a rural area may aid built heritage management, promoting projects aimed at its valorisation and, more generally, environmental safety. This could contribute to the improvement of air quality and, consequently, the health of people and monuments.

2. Site and Monument

This study presents the black crust and its components from the historic stones of Lipowiec Castle, situated in the village of Babice, Chrzanów county, in the Małopolska province (southern Poland). The castle, built in the 13th–15th centuries and subsequently seriously damaged by two 17th-century fires, was finally ruined in the 19th century. Since the 1950s, the picturesque castle ruin on the top of the limestone Lipowiec hill (362 m asl), covered with mature beech forest, has been legally protected as the Lipowiec Nature Reserve, extending over an area of 11.39 ha [36].

The Lipowiec hill, situated in the SW part of the Tenczyński Hump, close to an important fault stretching E–W and separating it from the Vistula River valley, consists of various Triassic limestones, partly dolomitised, in the upper part of the profile [37,38]. Lithologically, these include porous limestones from the Rhetium (the uppermost lower Triassic) and middle Triassic (known as 'Muschelkalk') wavy laminated and organogenic limestones, as well as ore-bearing and organogenic, diplopora dolomites outcropping nearby [37,39,40]. Direct observations of stone blocks within the castle walls allowed us to identify practically all varieties of the above-mentioned Triassic limestones and dolostones (Figure 1). During the complex renovation and conservation work in the 1960s and 1970s,

before opening the Lipowiec Castle ruin to the public, white Jurassic limestones of superior quality and resistance parameters, along with bricks, were added to the castle walls.

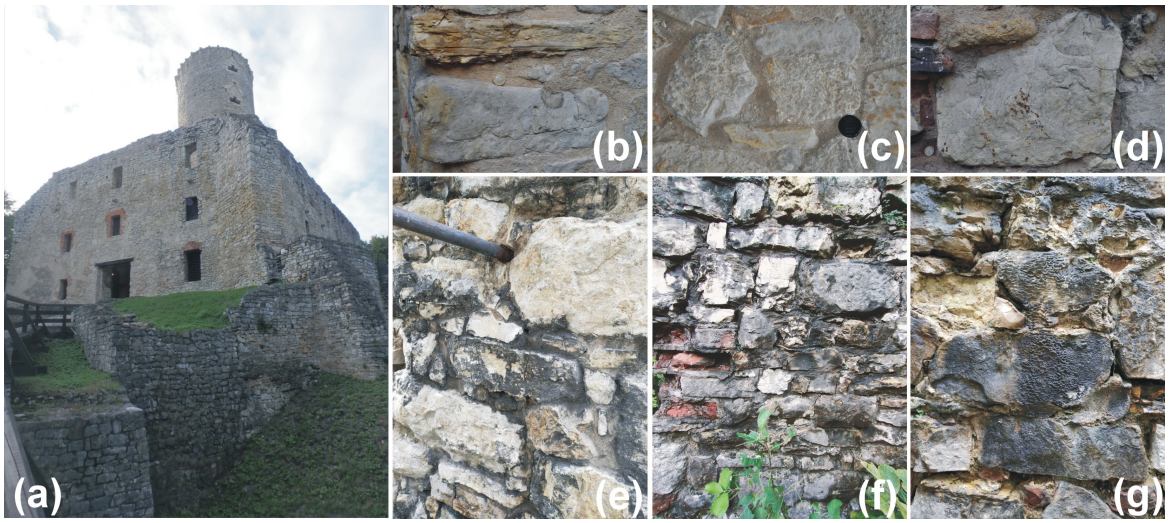

Figure 1. General view of the Lipowiec Castle after conservatory work in 2022–2023 (**a**). Examples of stones used for the construction of the castle, post-conservation: Triassic, wavy laminated limestone (**b**), Triassic organogenic dolomite (**c**), and ore-bearing dolomite (**d**). Signs of deterioration, black crust, and soiling on stone blocks and bricks before conservation (**e**–**g**).

The castle ruin is directly exposed to external factors, such as changing weather conditions and the direct impact of air pollution. Hence, it suffers from significant dampness resulting in the crystallisation of water-soluble salts, visible in the form of efflorescences and the disintegration of some blocks. In areas sheltered from direct rainfall, black and dark crusts are clearly visible on the stone surfaces. Traces of biological activity from microorganisms can also be observed. Some stone blocks exhibit more severe damage; they are cracked throughout, which results in settling and falling off the wall.

Lipowiec Castle, along with the village of Babice, is situated in the western part of the Małopolska voivodeship, halfway between the city of Kraków (35 km east) and the industrial region of Upper Silesia to the west. Although the immediate vicinity of the castle is a rural area, the whole Cracovian-Silesian region is one of the most polluted in Poland. The industrial towns of Oświęcim, Libiąż, Chrzanów, Trzebinia, and Olkusz lie only about 5–20 km W, NW, and N from the castle. Since the 19th century (even earlier in the case of Zn-Pb ores exploitation and smelting), the industrial development of the region has been based on mining, metallurgy, energetics, and chemical and metal industries. The area of Babice and Lipowiec may be affected by emissions from Zn-Pb ores exploitation (permanently halted in 2021), their processing, and smelting (still operational) in nearby Bolesław. With prevailing W and NW winds, the study area is exposed to substantial atmospheric pollution from the entire highly industrialised Upper Silesian Industrial Region, 30–60 km to the west. Even long-distance transport of contaminants from southern Upper Silesia, as well as Karvina and Ostrava in Czechia, about 100 km SW, cannot be ruled out. Possible industrial pollution from the Kraków agglomeration in the east should also be considered. Finally, local coal combustion of household fuels in the heating season, transport, and minor economic activities also contribute to the total air pollution in the study area. It should be noted that in the last three decades, harmful industrial activity in the region, as the case across Poland, has substantially decreased. Concurrently, the emission of pollutants is limited by strict EU and Polish legal regulations. On the other hand, the black crust on the surface of the Lipowiec Castle stones must have started to form during the onset and peak of the industrial activity in the region, several decades ago. Therefore, its study should yield valuable information on the nature of industrial pollution in a rural area, but in proximity to highly industrial and densely populated centres.

3. Materials and Methods

Samples were collected during the most recent castle conservation campaign in 2022, courtesy of Ms Karolina Pachuta from the Conservation and Renovation Company Piotr Białko Ltd., Kraków, Poland. They were taken from the west, south, and north wings of the castle ruin, at a height of about 1–1.5 m above ground level, with three or four samples from each side. At the time of sampling, the eastern part of the ruin was inaccessible for security reasons. The samples represent black crust and surface soiling formed on three types of building materials: limestone, dolomitic limestone and/or dolomite, and brick used in the construction and earlier renovations of the castle (Figure 1).

The black crust samples collected could be divided into two categories: larger ones, up to 20–30 mm, with a piece of stone or brick underlying a black crust (or very thin soiling only); and very small pieces of a black crust scaled off. In the first case, it was possible to make polished thin sections, cut perpendicular to the outer layers of the samples. These thin sections allowed for preliminary mineralogical and petrographic observations of stones and the determination of mineralogical composition and evaluation of the thickness of the black crust. They were also used for the SEM-EDS analysis.

For the preliminary microscopic analysis of stones, bricks, and black crust an Olympus BX-51 polarising microscope was utilised. Laboratory studies comprised extensive mineralogical and chemical analyses of the samples based on the following methods: Raman micro-spectroscopy (RS) and scanning electron microscopy coupled with energy-dispersive X-ray spectroscopy (SEM-EDS).

The molecular characteristics of the particulate matter were determined using Raman micro-spectroscopy. The spectra were recorded with a Thermo Scientific DXR (Data Extraction and Recording) Raman Microscope with a 900 grooves/mm grating and a charge-coupled device (CCD) detector. The Olympus 10× (NA 0.25) and 50× (NA 0.50) objectives (theoretical spot sizes of 2.1 and 1.1 μm, respectively) were used. A 532-nm diode laser (with a maximum power of 10 mW) was the excitation source. The spectra were recorded at an exposure time of 3 s and from ten to hundred data accumulations. The laser power varied from 3 to 10 mW, depending on the quality of spectra, to avoid possible thermal decomposition of the material analysed. Band component identification was performed using the Omnic software package (Omnic 9, 1992–2012, Thermo Fisher Scientific Inc., Waltham, MA, USA). The spectra were analysed based on free Raman databases (e.g., RRUFF Raman Minerals spectra libraries [41]) and other literature data [42–44]. They were recorded randomly on the crust samples under study. In addition, Raman line maps across the samples were acquired, using the computer-controlled x–y–z stage. The line consists of ca. 100 spectra at a step size of 5 μm. All the obtained spectra have been analysed.

The morphology, microstructure of the crusts, and elemental composition of their components were studied using a Field Electron and Ion Company (FEI) 200 Quanta FEG (field emission gun) scanning electron microscope with an EDS/EDAX spectrometer (FEI Company, Fremont, CA, USA, AMETEK (GB), EDAX Business Unit, Leicester, UK). The maximum excitation voltage was 20 kV and a low vacuum mode (with a pressure of 60 Pa) was used. Analyses were conducted on relatively flat pieces of the exposed and slightly altered black or dark crusts. Large numbers of standardised analytical points were used to characterise the particulate matter present within the crust samples. Characteristics of anthropogenic particles on the crust surface were based on semiquantitative chemical composition. Mapping of selected microscopic areas in the samples, demonstrating the distribution of selected elements over the crust surface, was also performed. Selected samples were examined in profiles perpendicular to the weathered surfaces (thin sections).

Raman micro-spectroscopy (RS) and scanning electron microscopy with energy-dispersive spectrometry (SEM-EDS) were chosen as they allow analysis of individual particles embedded within the black crust. Moreover, even very small, millimetre-sized samples could be examined, which is very important for historical objects. Restrictions in sampling stone monuments and minimising sample dimensions often limit a comprehensive application of other analytical methods, making the clarity of results rather problematic.

At the same time, non-destructive RS and SEM-EDS permit to use of the same samples for both analytical methods, yielding information about the elemental and molecular composition of the black crust components. They also enable the visualisation of the distribution of the crust components based on relevant maps. Finally, Raman spectroscopy allows us to distinguish secondary salts of various hydration degrees, which are very deleterious, as they substantially change their volume in dissolution–recrystallisation cycles. The crystallisation pressure resulting is one of the most effective damaging factors [12,45].

4. Results

4.1. Raman Micro-Spectroscopy

Spectra of carbonaceous particles, presumably soot, were recorded for black crust developed on limestone, dolomitic limestone, dolomite blocks, and bricks. Typical first-order Raman spectra collected in this study are presented in Figure 2. The spectra exhibit two broad bands that peak within 1350–1380 cm^{-1} (D peak, i.e., Defect peak) and between 1580 and 1650 cm^{-1} (G peak, i.e., Graphite peak). This indicates the presence of both nanocrystalline and amorphous carbon. As the ratio of the areas of the D and G bands (ID/IG) serves as an indicator of disorder in the graphite lattice, spectral parameters from two-band curve-fitting procedures, often used for carbonaceous particles [46–48], could be determined. The ID/IG ratio decreases with increasing order in the structure of the carbonaceous matter [49–51]. However, the ID/IG ratio also depends on the carbon nanostructure, whether it leans towards an amorphous layered carbon or disordered nanocrystalline graphitic carbon. Existing sources report that for nearly amorphous carbon films, the ID/IG ratio increases with increasing dimensions of the graphite crystallites [52,53]. On the other hand, for disordered nanocrystalline graphitic carbon, the ID/IG ratio decreases with increasing sizes of the graphite crystallites [48,54].

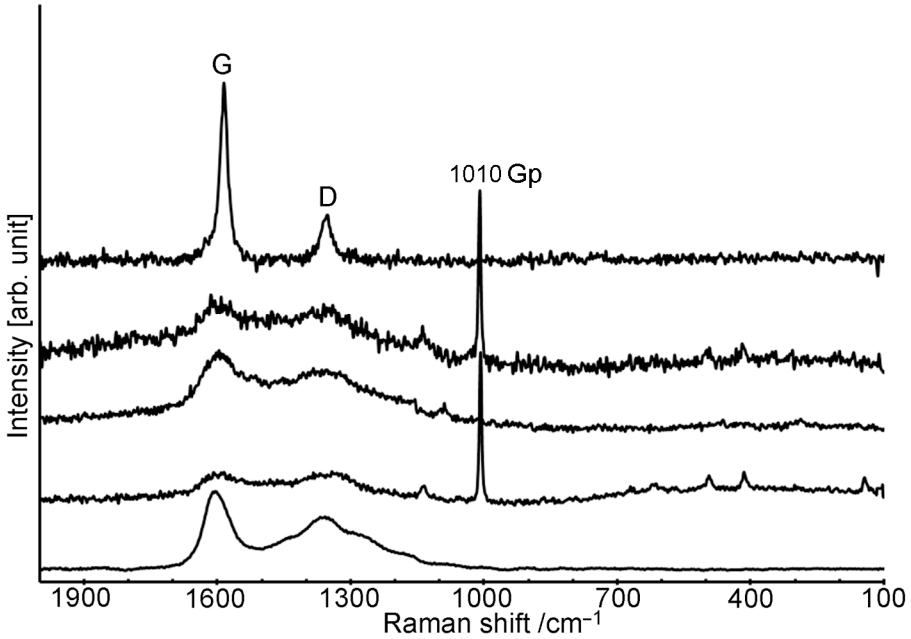

Figure 2. Representative first-order Raman spectra of carbonaceous matter, presumably soot (bands G—Graphite peak, and D—Defect peak), from black crust samples. The spectra also display a band characteristic for gypsum (Gp, main band at 1010 cm^{-1}).

The spectra produced in this study were fitted with a combination of G and D bands at ~1600 or ~1585 and ~1360 cm^{-1}, respectively. It was found that the analysed carbon particles exhibited different values of the ID/IG ratio. Generally, two groups of soot could be observed. One group is characterised by a higher ID/IG ratio in the range of 3.55–4.03, while for the other, these values are significantly lower, in the range of 0.29–0.65. This may

suggest various structural disorders in soot; e.g., ID/IG for graphite of a solid electrode bar is 0.2, whereas for highly ordered SHER graphite it is 0.0 [49]. In one of the author's previous studies on graphitic carbon from the black crust on the historic monuments in Kraków (Poland), these ratios reached 1.3 [55].

A typical Raman line map of the black crust covering the stone blocks is presented in Figure 3. The distribution of amorphous carbon on the black crust surface is characterised by the presence of G and D bands in the spectrum (a single peak area option between 1350 and 1650 cm^{-1} was applied), the line consists of ca. 100 spectra at a step size of 5 µm. The varying intensity of Raman bands in the line map seems to indicate that carbonaceous particles do not form a compact layer. In the selected range, some bands related to β-carotene could also be identified [56]. However, due to overlap with soot bands, this substance could be detected only in a few points of the profile. It may be inferred that the graph corresponds to the presence of soot in the sample along the profile analysed.

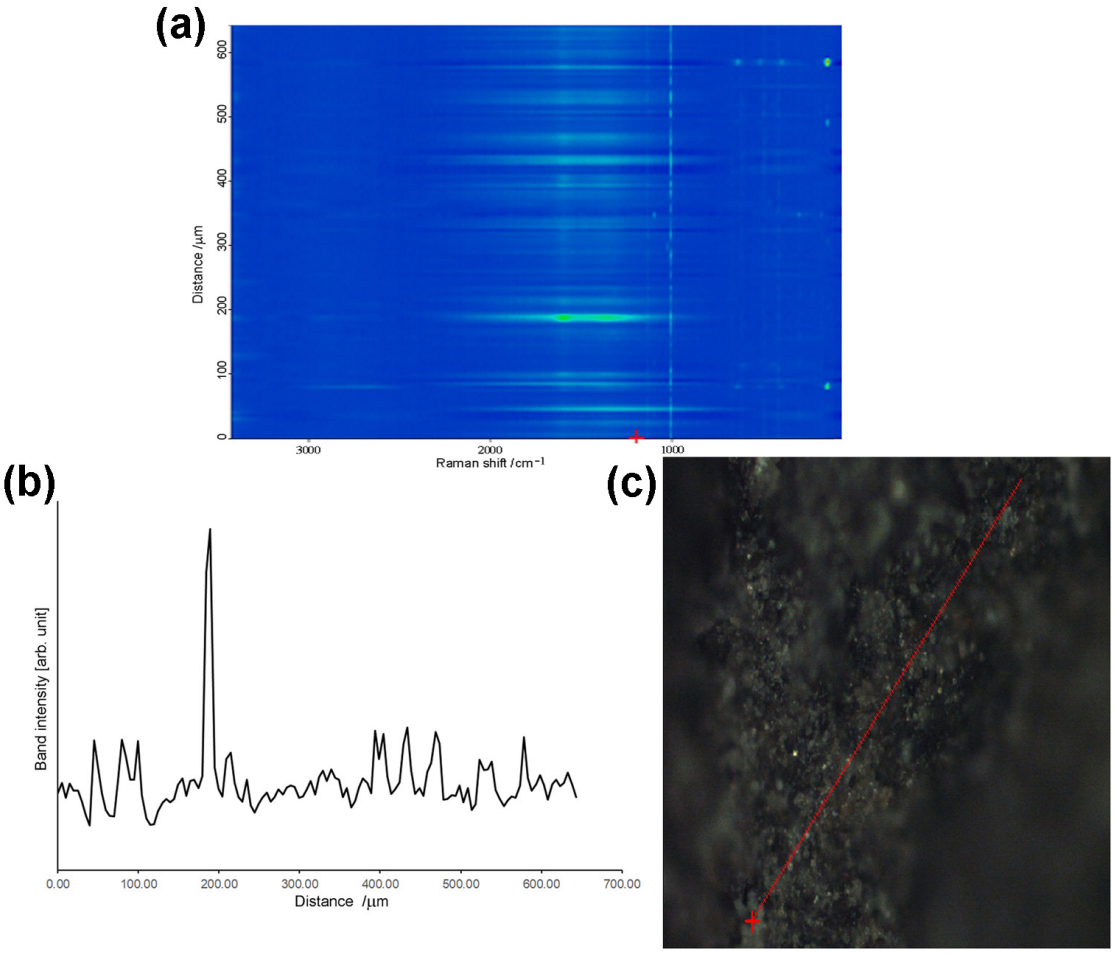

Figure 3. Distribution of amorphous carbon on the black crust surface based on Raman microspectroscopy analyses. Images of resulting Raman signals as a 2D map (Raman intensity in terms of blue colour brightness) (**a**), line map (peak area range between 1350 and 1650 cm^{-1} versus distance) (**b**), and photomicrograph of black crust with analytical profile (dotted line; "+" starting point of the profile) (**c**). Image (**a**) indicates the presence of gypsum (thin vertical line ~1100 cm^{-1}).

Other black crust components are salt minerals. In the case of the crust developed on building materials from Lipowiec Castle, sulphate salts predominate. A common and typical secondary mineral of the black crust is gypsum ($CaSO_4 \cdot 2H_2O$), which was detected in the crusts formed on limestone, dolomitic limestone, dolomite blocks, and bricks. The presence of this mineral was confirmed by the bands at 1010 cm^{-1} (ν_1 symmetric stretching), minor bands at 416 and 492 cm^{-1}, in addition to 621 and 672 cm^{-1} (ν_2 symmetric

and ν_4 antisymmetric bending of SO_4^{2-}, respectively) and 1136 cm^{-1} (ν_3 antisymmetric stretching) [50,57] (Figure 4a). Its presence, marked with a line ~1100 cm^{-1}, is also evident in the Raman line map (Figure 3).

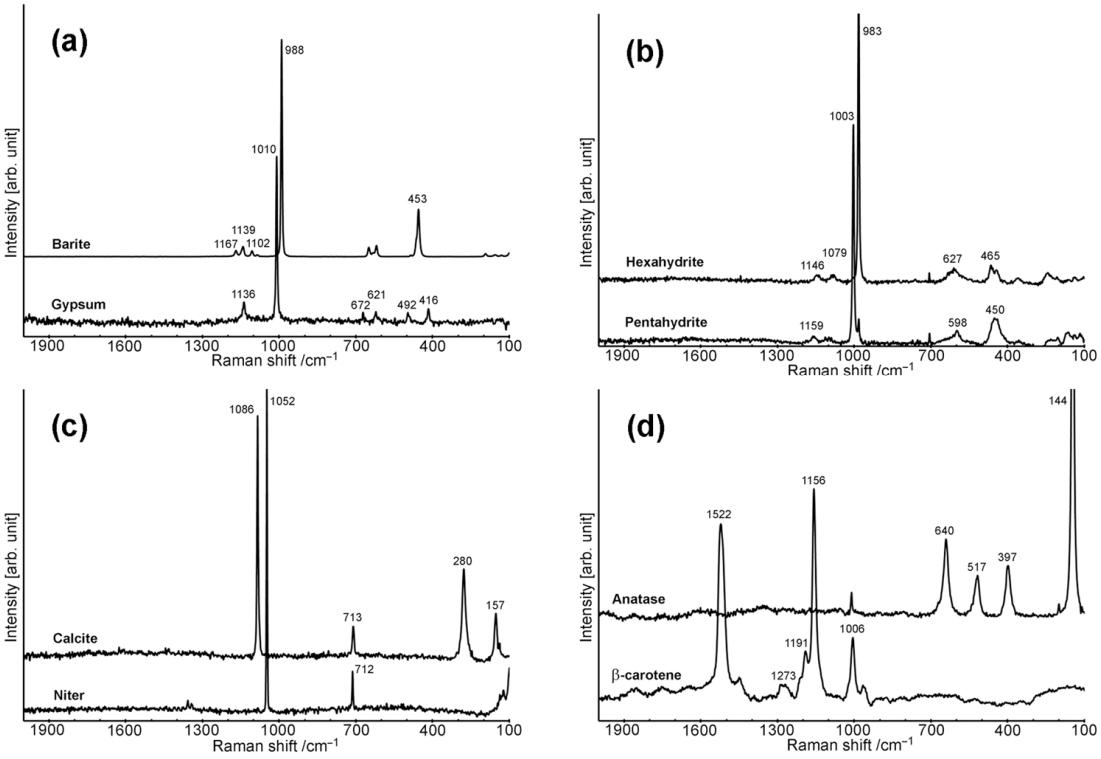

Figure 4. Characteristic Raman spectra of secondary salt minerals from the black crust samples: gypsum and barite (**a**), pentahydrite and hexahydrite (**b**), niter and calcite (**c**), and β-carotene and anatase (**d**).

In addition to gypsum (hydrated calcium sulphate), in crust samples covering dolomitic limestone, dolomite blocks and bricks, hydrated magnesium sulphates ($MgSO_4 \cdot nH_2O$ series) were occasionally detected (Figure 4b). Primarily, however, they occur in the form of efflorescences, not as a component of the black crust. Shifts of the major SO_4^{2-} Raman band (ν_1) and the position of the bands around 1050–1200 cm^{-1} (ν_3 SO_4^{2-}) helped to determine the degree of hydration of these phases [42]. The Raman spectra with the signals at 1146 (ν_3), 1079 (ν_3), 983 (ν_1), 627 (ν_4), and 465 (ν_2) cm^{-1} correspond to hexahydrite $MgSO_4 \cdot 6H_2O$ [42,43]. However, in the absence of a ν_3 SO_4^{2-} band, the presence of epsomite $MgSO_4 \cdot 7H_2O$ cannot be excluded (ν_1 at 983 cm^{-1}). Furthermore, the bands at 1159 (ν_3), 1003 (ν_1), 598 (ν_4), and a shoulder ca. 450 (ν_2) should be attributed to pentahydrite $MgSO_4 \cdot 5H_2O$ [42,43].

Another salt occasionally detected in the black crust on carbonate building stones is barite ($BaSO_4$) (Figure 4a). Its occurrence is confirmed by the intensive band at 988 (ν_1) cm^{-1} and other characteristic absorption bands: ν_2 bands at 453 and 461 cm^{-1}; ν_3 bands at 1102, 1139, and 1167 cm^{-1}. Additionally, the presence of niter KNO_3 could be inferred from its main bands at 1052 cm^{-1} and 712 cm^{-1} (Figure 4c). This salt was found on both stone blocks and bricks.

Occasionally, calcite has been observed on the black surfaces of bricks and even as a white crust on some bricks. Its presence is evidenced by bands at 1086, 713, 280, and 157 cm^{-1} (Figure 4c).

The previously mentioned carotenoids, registered in the black crust covering the stone blocks (Figure 4d), should indicate the presence of microorganisms producing these organic pigments in the crust. The bands recorded at 1006, 1156, 1191, 1273, and 1522 cm^{-1} allow the identification of β-carotene [56,58].

Furthermore, the bands at 144, 397, 517, and 640 cm^{-1} are associated with the presence of anatase (β-TiO_2) (Figure 4d). TiO_2 particles were found among the components of all the analysed black crust samples.

4.2. SEM-EDS

Scanning electron microscope observations and analyses of the black crust samples confirmed the presence of the phases identified by the Raman micro-spectroscopy and allowed the detection of other particles deposited on the exposed stone surfaces.

The black crust on both stone blocks and bricks was composed of gypsum, and in some samples, it was accompanied by other salts, such as hydrated magnesium sulphates, niter, and single crystals of barite. The gypsum layer is up to about 200 µm thick (Figure 5). Gypsum crystals are subhedral and/or anhedral in shape and sometimes they exhibit signs of dissolution. Magnesium sulphates and niter, occasionally present in black crust developed on dolomitic limestones, dolomites, and bricks, exhibit anhedral habits. Barite, present in crust developed on blocks of carbonate rocks, forms irregular crystals with sharp edges, up to 5 µm in size. Gypsum crystals form a type of network, in which various solid particles are entrapped. The EDS maps present the distribution of Ca, Mg, and S, indicating the quantitative domination of sulphate phases. The distribution of Si, Al, Fe, and Ba demonstrates the presence of various chiefly anthropogenic particles embedded in the sulphate matrix (Figures 5 and 6).

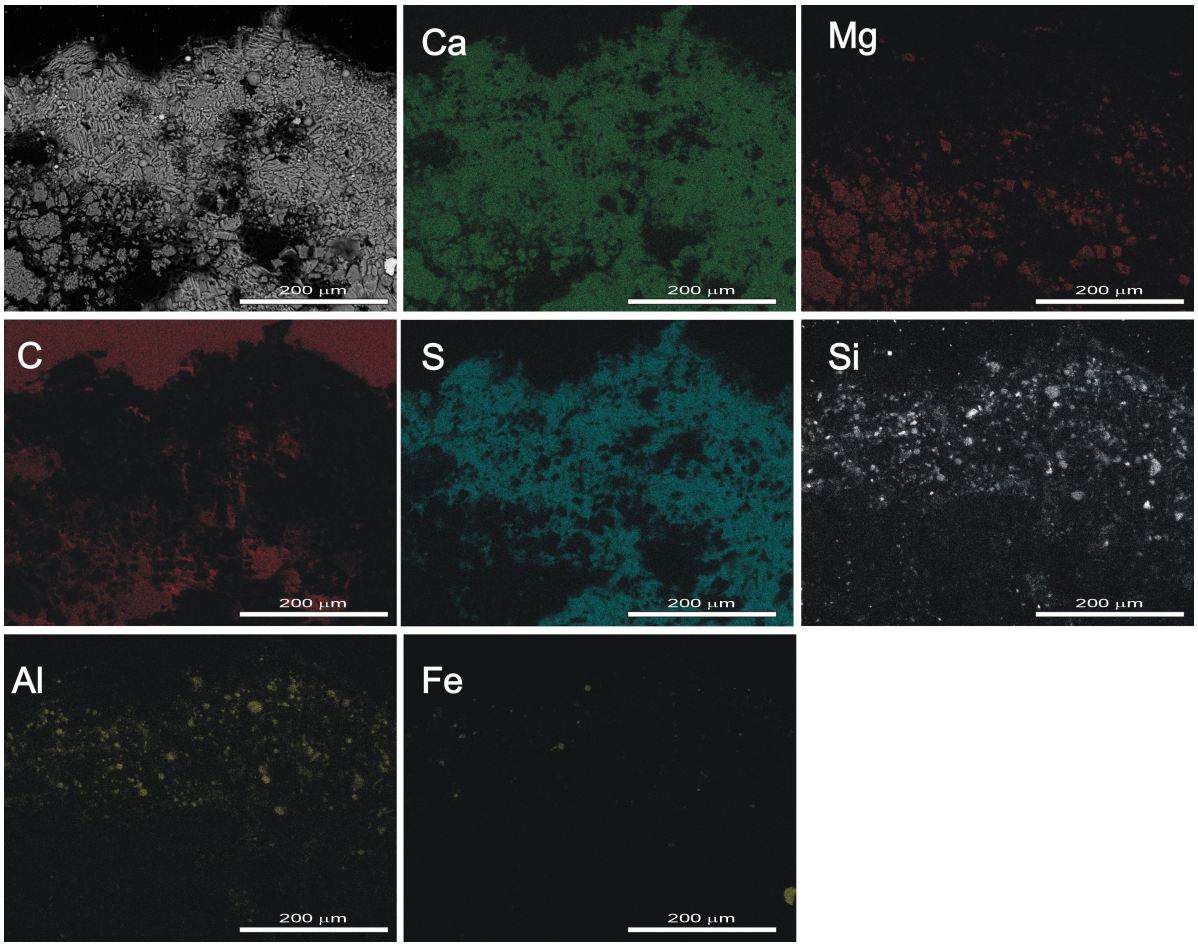

Figure 5. EDS elemental distribution maps of Ca, Mg, C, S, Si, Al, and Fe. Sample of the dolomitic limestone; thin section cut perpendicular to the surface.

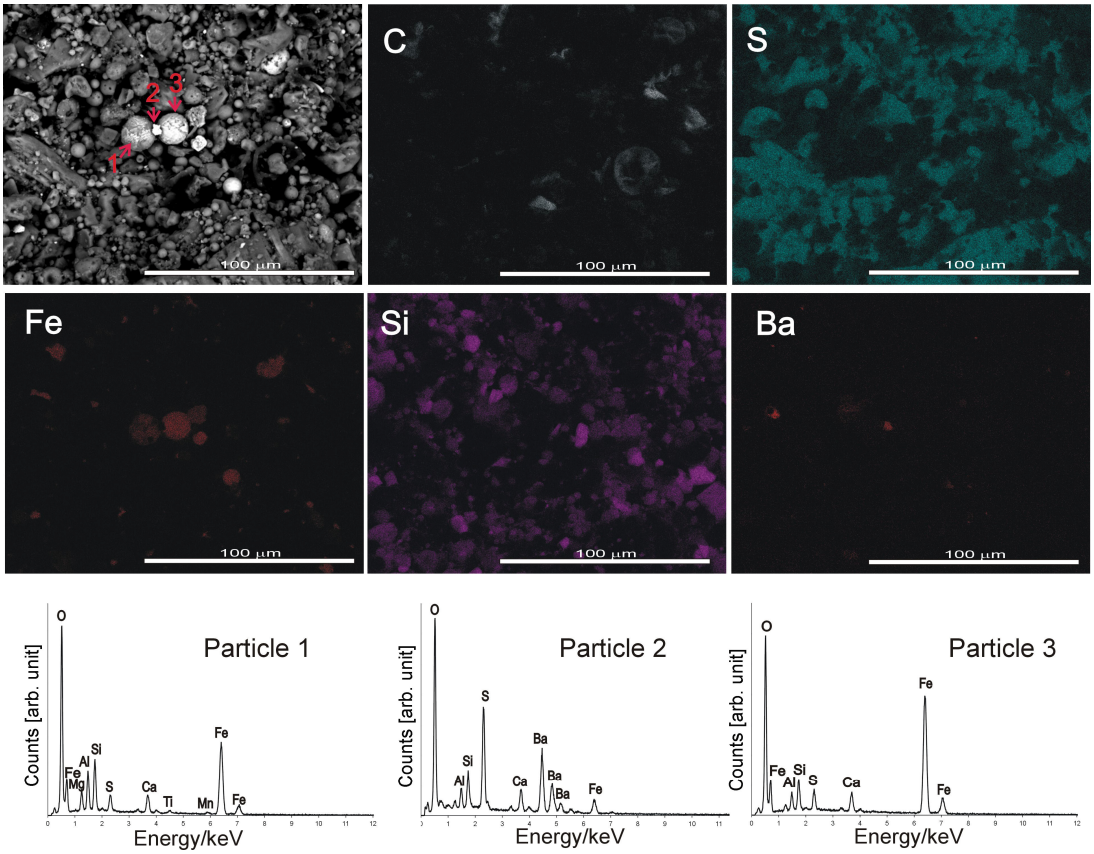

Figure 6. EDS elemental distribution maps of C, S, Fe, Si, and Ba, and elemental composition of anthropogenic particles visible at the back-scattered electron (BSE) image of the black crust. The image presents spherical iron oxide particles with dendritic surfaces (1, 3) and a particle of barium sulphate (2) dispersed among other anthropogenic particles and gypsum crystals. The semiquantitative composition of particles 1–3 is provided in Table 1.

Table 1. Semiquantitative composition (weight %) of particles deposited on the black crust, acquired using EDS. For the exact positions, appearance, and shapes of the particles analysed, see Figures 6–9.

	Analysed Point *														
Element	**1**	**2**	**3**	**4**	**5**	**6**	**7**	**8**	**9**	**10**	**11**	**12**	**13**	**14**	**15**
C	5.98	7.47	5.66	5.43	26.52	25.96	5.22	4.03	5.51	4.16	69.79	50.84	4.77	4.73	4.58
O	41.11	38.84	34.24	45.51	41.78	32.37	37.51	40.59	18.96	36.81	20.20	16.14	47.00	43.92	40.27
Na	b.d.l.	b.d.l.	b.d.l.	0.69	0.39	b.d.l.	b.d.l.	0.24	0.19	b.d.l.	0.28	b.d.l.	b.d.l.	b.d.l.	b.d.l
Mg	3.30	0.98	1.12	1.22	0.58	0.24	0.56	1.81	0.77	1.20	0.21	b.d.l.	2.56	0.49	0.51
Al	5.49	2.37	2.45	14.74	10.94	6.47	1.44	1.86	1.79	1.96	0.64	b.d.l.	2.28	1.19	1.35
Si	6.09	3.44	3.49	23.50	12.24	10.88	3.31	2.61	2.81	3.55	1.14	0.92	7.59	2.12	2.66
P	0.34	b.d.l.	0.29	b.d.l.	b.d.l.	b.d.l.	b.d.l.	0.l8	b.d.l.	0.33	b.d.l.	b.d.l.	0.60	b.d.l.	b.d.l.
S	2.03	9.73	2.17	0.89	1.62	1.82	1.86	3.10	6.79	3.55	2.71	2.83	4.78	6.60	6.65
Cl	b.d.l.	b.d.l.	b.d.l.	b.d.l.	b.d.l.	b.d.l.	b.d.l.	b.d.l.	b.d.l.	b.d.l.	b.d.l.	b.d.l.	b.d.l.	b.d.l.	b.d.l.
K	0.49	0.50	0.47	2.89	1.28	2.03	0.45	0.23	0.57	0.42	0.77	b.d.l.	0.73	0.33	0.41
Ca	2.77	2.66	2.60	1.93	3.65	3.85	2.96	4.62	8.37	5.79	3.19	3.71	9.04	7.67	7.06
Ba	b.d.l.	29.02	b.d.l.	b.d.l.	b.d.l.	b.d.l.	b.d.l.	b.d.l	b.d.l.	b.d.l.	b.d.l.	b.d.l.	b.d.l.	b.d.l.	b.d.l.
Ti	0.59	b.d.l.	b.d.l.	0.51	0.34	b.d.l.	b.d.l.	0.13	0.38	b.d.l.	b.d.l.	b.d.l.	0.56	b.d.l.	0.32
Cr	b.d.l.	b.d.l.	b.d.l.	b.d.l.	b.d.l.	b.d.l.	0.64	b.d.l	26.77	b.d.l.	b.d.l.	b.d.l.	0.50	b.d.l.	0.22
Mn	0.61	b.d.l.	b.d.l.	b.d.l.	b.d.l.	b.d.l.	b.d.l.	0.71	0.91	0.59	b.d.l.	b.d.l.	3.17	b.d.l.	0.17
Fe	31.21	4.97	47.64	2.63	0.69	0.85	46.04	39.90	26.10	40.67	1.06	6.29	14.26	31.77	33.54
Co	b.d.l.	b.d.l	b.d.l	b.d.l	b.d.l	b.d.l	b.d.l	b.d.l	b.d.l	b.d.l	b.d.l	0.17	b.d.l.	b.d.l.	b.d.l
Cu	b.d.l.	b.d.l.	b.d.l.	b.d.l.	b.d.l.	0.32	b.d.l.	b.d.l	b.d.l.	b.d.l.	b.d.l.	b.d.l.	1.15	1.17	1.41
Zn	b.d.l.	b.d.l.	b.d.l.	b.d.l.	b.d.l.	3.53	b.d.l.	b.d.l	b.d.l.	0.98	b.d.l.	b.d.l.	1.01	b.d.l.	0.79
As	b.d.l.	b.d.l.	b.d.l.	b.d.l.	b.d.l.	b.d.l.	b.d.l.	b.d.l	b.d.l.	b.d.l.	b.d.l.	19.11	b.d.l.	b.d.l.	b.d.l.
Pb	b.d.l.	b.d.l.	b.d.l.	b.d.l.	b.d.l.	11.42	b.d.l.	b.d.l	b.d.l.	b.d.l.	b.d.l.	b.d.l.	b.d.l.	b.d.l.	b.d.l.

* For the exact positions of the analysed particles, see Figures 6–9. b.d.l.—below the detection limit. The detection limit is about 0.1 wt%.

Analyses of single grains, their shapes, and chemical composition determined by EDS allow for the classification of these particles. Carbonaceous particles, likely soot, giving a dirty, black appearance to the stone surface, are dispersed among the crust components, without forming a uniform, continuous layer. The SEM-EDS map of the surface distribution of carbon, displayed in Figure 6, is consistent with the results based on Raman microspectroscopy analyses (see also Figure 3). Soot particles form aggregates usually elongated in shape, up to ca. 20 µm. Individual grains composing such aggregates were not distinguishable enough to be analysed separately. The most detailed structural characteristics of soot could be achieved by, for example, high-resolution transmission electron microscopy.

Other commonly observed components of the crust are fly ash particles. These anthropogenic components are chiefly represented by smooth, spherical aluminosilicate glass particles, ranging from several to 20–30 µm in size. The principal chemical components of the glass spheres are silicon (Si) and aluminium (Al), accompanied by calcium (Ca), potassium (K), magnesium (Mg) and, in some particles, admixtures of iron (Fe) and titanium (Ti) (Figure 7, Table 1). The particles are partially covered by small crystals of calcium sulphate, presumably gypsum (Figure 7), which may suggest favourable conditions for sulphate crystallisation. Apart from the above elements, spherical particles containing Pb and Zn, up to 5 µm in size, have also been encountered (Figure 7, Table 1).

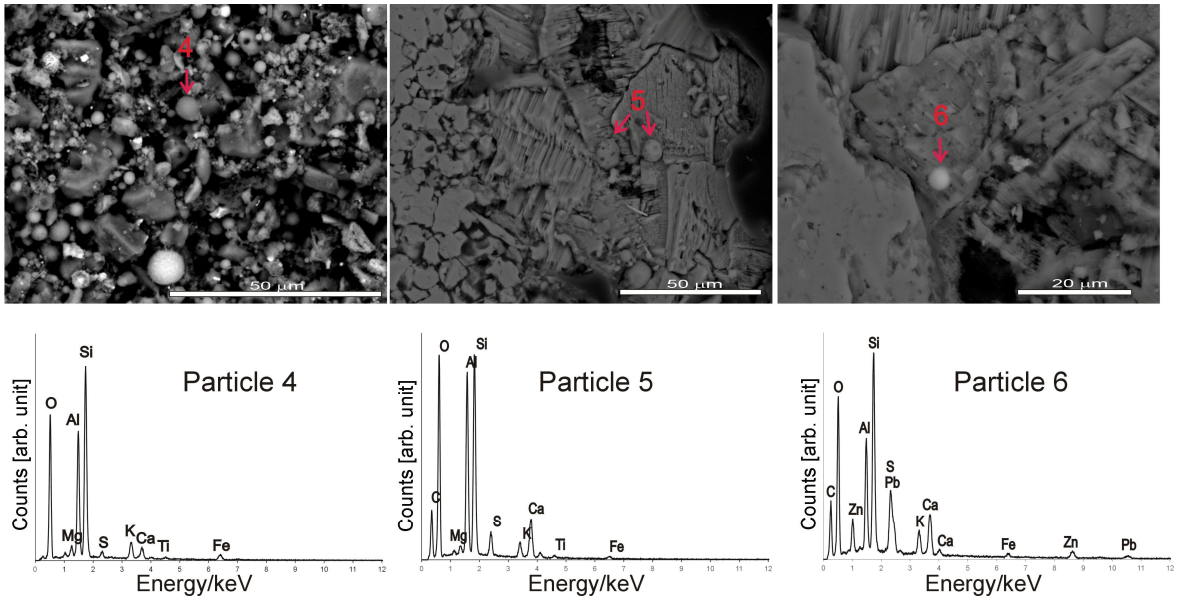

Figure 7. Back-scattered electron (BSE) images of the black crust and elemental composition of anthropogenic particles marked on the images. Spherical aluminosilicate glass particles of various compositions (4–6) are visible. Particle 4 is partly covered with small crystals of calcium sulphate, likely gypsum, which may indicate favourable conditions for sulphate crystallisation on its surface. The semiquantitative composition of particles 4–6 is provided in Table 1.

Fairly abundant spherical particles of iron oxides, from several to a few dozen µm in size, exhibited smooth (Figures 8 and 9) or characteristic dendritic (Figures 6 and 8) morphology of their surfaces. Their main component is Fe, whereas Mn, Ti, Zn, and Cr are present as admixtures (Figures 6, 8 and 9 and Table 1). Iron oxide particles generally contain only small, subordinate amounts of glassy matrix.

Irregular and sharp-edged particles were also observed, up to 10 µm in size, containing such metals as Fe, Cr, As, Mn, Co, Cu, and Zn (Figures 8 and 9 and Table 1).

Silicates, among them quartz and feldspars (alkali feldspars $KAlSi_3O_8$ and $NaAlSi_3O_8$), were also identified as particulate matter deposited on stone surfaces.

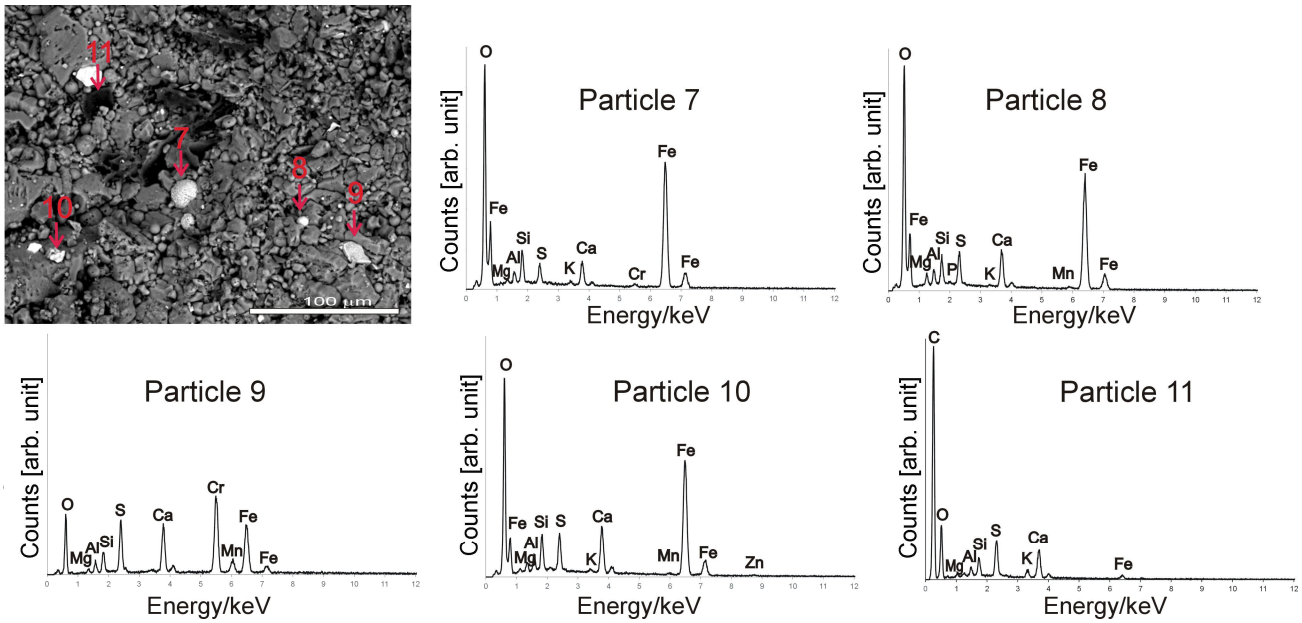

Figure 8. Back-scattered electron (BSE) image of the black crust and elemental composition of some particles are marked on the image. The image presents spherical particles of iron oxide of various morphology and composition (7–8), sharp-edged shaped particles enriched in heavy metals (9–10), and a carbonaceous particle (11) trapped in a gypsum matrix. The semiquantitative composition of particles 7–11 is provided in Table 1.

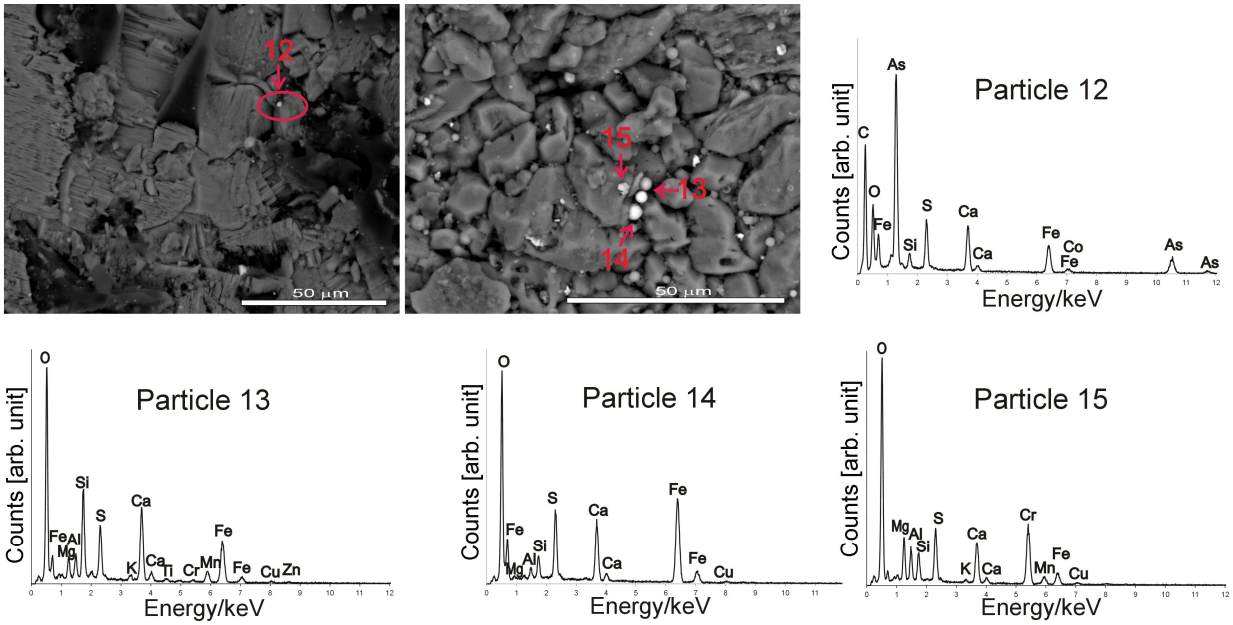

Figure 9. Back-scattered electron (BSE) images of the black crust and elemental composition of some particles, marked on the image. The images present irregular particles containing heavy metals (12, 15) and spherical particles enriched in iron and other metals (13, 14) among gypsum crystals. The semiquantitative composition of particles 12–15 is provided in Table 1.

5. Discussion

Based on the RS and SEM-EDS analyses, black crust samples from various stone blocks and bricks, collected from different parts of the castle ruin, were found to be quite uniform in their chemical and phase composition. This lack of significant variability, depending on geographic and prevailing wind directions, is presumably due to the proximity of multiple

sources of pollution in the region. The black crust on stones and bricks consists of a gypsum matrix with carbonaceous matter, likely soot, and other anthropogenic particles entrapped among the sulphate crystals. According to the literature, this is a characteristic feature of black crust [20,22].

Major sources of soot emissions include transportation, industry, individual households (for heating and cooking), and open burning. In small towns and villages in Poland, household coal combustion is still a major source of soot, particularly in the autumn and winter seasons. Nevertheless, the origin of the soot particles is difficult to determine. Their morphology, sizes, and shapes vary, depending on type of the fuel burned, combustion processes (temperature, cooling rate of the exhaust gases), and chemical reactions in the atmosphere [59]. Raman micro-spectroscopy analyses provided significant data for the characteristics of these particles. Based on these analyses, the observed variations in the ID/IG area ratio calculated (ID/IG ratios in the ranges of 3.55–4.03 and 0.29–0.65) reflect different sources of carbonaceous matter. A study of the airborne ambient soot (PM 2.5) collected at suburban air monitoring stations in southern Poland (Silesia province) revealed that the ID/IG area ratio is distinctly higher for samples from the heating season than for these from the non-heating part of the year, mirroring the ID/IG ratio for soot originating from coal combustion and wood burning. On the other hand, values for the non-heating season samples are close to the ID/IG area ratio of diesel soot [60]. In the case presented, the anthropogenic particles observed on the black crust surface, including soot, have been deposited over an extended period, most likely since the last major conservation campaign in the 1970s. Therefore, they should reflect the long-term aerosanitary condition of the area. The variations in the ID/IG ratio indicate the presence of both soot from coal or wood combustion and transportation-related emissions deposited over the years.

A more detailed analysis of the carbonaceous matter, using a five-band combination (G, D1, D2, D3, D4) after deconvolution of the Raman spectrum, enables the determination of additional parameters. These include the full width at half maximum (FWHM) of the D1 and ID/IG bands, among others [49–51], which characterise carbon particles. The degree of graphitic structural ordering in soot increases as the width of the D1 band decreases. Moreover, as suggested by Soewono and Rogak [48], plotting the ID/IG relationship against the D1 FWHM may facilitate the separation of particles into different clusters, giving a broader view of the diversity of carbonaceous matter.

The fly ash particles, commonly present in the crusts analysed, are mostly spherical aluminosilicate glass particles, with other metals such as Ca, K, Mg, Fe, and Ti, and occasionally Pb and Zn, in their chemical composition. Al-Si glass spheres are characteristic products of high-temperature combustion of solid fuels. Fly ash is produced by coal-fired power and steam-generating plants and individual heating furnaces. In the black crust, Al-Si glass spheres are a molten mineral residue of coal (the composition of these smooth particles is akin to that of clay impurities in coal), which, in the case of power plants, were not removed by particulate emission control devices and thus entered the air. However, an important part of such contaminants in the region discussed may be due to local emissions related to individual heating. The chemical composition of the pollutants emitted into the atmosphere from household coal combustion varies, depending on both the physical and chemical parameters of the hard coal burned and the combustion technology [61]. Elements such as As, Cd, Pb, Ni, Zn, and Cu occur in hard coal accessory minerals (such as pyrite, sphalerite, galena, magnetite, and hematite). During combustion, they concentrate on solid products and are emitted into the atmosphere along with dust [62]. Therefore, the presence of Pb and Zn in the Al-Si spheres may be linked to the hard coal combustion processes.

On the other hand, mining and processing of Pb and Zn ores in the neighbouring Olkusz area (ca. 20 km to N), may be a more important source of such particles. Vast Zn-Pb deposits, of the Mississippi Valley type, have been exploited for centuries, until the closure of the last mine in 2021. The Triassic ore-bearing dolomites contain primary sulphides (ZnS—sphalerite, PbS—galena, FeS_2—pyrite and marcasite) and secondary Zn and Pb minerals, including oxides, carbonates, sulphates, silicates, etc. [63,64]. Besides Zn, Pb, and

Fe, these ores contain minor or trace amounts of other heavy metals (Mn, Cd, Tl, Ag) and metalloid elements (As, Sb) [64,65]. Ore enrichment and various metallurgical processes (roasting, melting, sintering, casting, and rolling) are all potential sources of harmful heavy metal emissions [66]. Although the plants use highly efficient dust collectors to curb the emission of pollutants into the air, dust particles, especially the finest ones, still manage to enter the atmosphere. These particles then settle on the earth's surface, contaminating soils, groundwater, and plants, eventually making their way into the food chain. In general, the chemical composition of dust from various iron and non-ferrous metallurgy processes is different. Jabłońska et al. [67] demonstrate that elements such as Fe, Mn, Cr, and V occur in significantly higher quantities in waste from iron metallurgy. The copper content in dust from both iron and non-ferrous metallurgy varies considerably, with higher levels observed in non-ferrous metallurgy. The content of zinc, lead, and especially cadmium is also higher for dust from non-ferrous metallurgical processes.

Other abundant crust components are spherical particles of iron oxides, exhibiting smooth or dendritic surface morphology. Crystallographic data acquired in one of the author's previous studies [68] using the electron back-scattered diffraction technique (EBSD) enabled the identification of most of these iron oxide particles as hematite. However, the dendritic surfaces of some particles may be related to the coexistence of hematite and magnetite. These two iron oxides often intergrow, indicating that the dendrites could initially have formed in the reducing part of the furnace as Fe_3O_4 and later oxidised to Fe_2O_3 [69,70]. Unfortunately, no spectra indicating the presence of hematite or magnetite were recorded during the Raman micro-spectroscopy analyses. This may be due to the very small dimensions of these particles, along with the phenomenon of fluorescence, which hampers the registration of spectra. The iron oxide particles are typical for emissions from the metallurgical industry, but they could also be associated with emissions from coal power plants [59]. Similarly, spherical particles and aggregates, with chemical composition comparable to all of those from the crust samples analysed in this study, were observed in the soils sampled near the Zn-Pb metallurgical plant in nearby Bukowno. In addition to small amounts of Si and Al, they also contain admixtures of Fe, Zn, Pb, Mn, Cd, and As [65,71]. The presence of these metallic elements confirms a large contribution of emissions from metallurgical processes to soil contamination.

The presence of irregularly shaped and sharp-edged particles enriched in heavy metals, such as Zn, Pb, Mn, As, and Fe, is mostly associated with emissions from the Zn-Pb industrial region of Olkusz and Bukowno. Their presence could also be due to the material itself, i.e., pieces of ore-bearing dolomite in the castle walls, with altered sulphide crystals (Figure 1d). However, their presence within the black crust, interspersed among the gypsum crystals, does not preclude their deposition with falling dust. This is further supported by their composition, which does not correspond to that of the ore minerals present in the rock. Unfortunately, metal deposition monitoring has not been carried out in this region for several years, but the results of measurements performed in the 1990s revealed the presence of these metals in the PM10 dust fraction [72].

It should be emphasised that the particles containing heavy metals discussed above are hazardous to human health due to their toxicity. They can enter the human body via the respiratory system. PM 2.5 can reach the alveolar parts of the lungs and directly enter the bloodstream. Epidemiological and toxicological studies have proven that exposure to these fine particles increases mortality and hospital admissions due to respiratory and cardiovascular diseases [73]. However, there is increasing evidence that coarse particles (>2.5 μm) could also cause adverse health effects [74]. Coarse particles are particularly abundant in areas with high road traffic, and/or high industrial emissions combined with relatively low precipitation.

The origin of other particles identified in the black crust analysed, like anatase and barite, should be considered in the context of both anthropogenic and natural sources. Particles of anatase (β-TiO_2), detected in all samples analysed, are likely to originate from cements and plasters, which are made with titanium white pigment to increase their

resistance to colour changes [75]. However, TiO_2 is also used as a support material for catalyst processes and as a component in asphalt pavement [76]. Aggregates of TiO_2 particles have previously been reported in the black crust on heritage buildings and in atmospheric particulate matter [55,59,77]. As this mineral is extremely rare in limestones, its presence as one of the substrate components can be ruled out.

Regarding barite particles, occasionally detected in the crust, their origin may be related to the limestone itself, which may contain isomorphic admixtures of barium. This element tends to accumulate in aragonite (a polymorph of $CaCO_3$) forming the skeletons and shells of marine invertebrates. Over time, aragonite transforms into calcite; however, barium concentrations in calcite are often lower than in aragonite [78]. Barite could also have formed through reactions between rock components and a polluted atmosphere. In dark, gypsum-rich crusts on limestone blocks, barite was also reported in previous studies on heritage stony buildings [55]. However, given the low levels of barium in fresh samples of quarried limestone [79], the rock itself may not be a sufficient source of this element. On the other hand, barium could have come from other sources as well. Among others, this element was intentionally introduced into building stones during previous restoration procedures. Barium chloride ($BaCl_2$) or barium hydroxide ($Ba(OH)_2$) are commonly used to remove harmful salts from stones and to consolidate the material [1]. Finally, the presence of barite crystals could result from inefficient burning of Ba-enriched coals (up to 4260 ppm Ba) for domestic purposes at temperatures of 800–900°C and subsequent emission of unmolten barite [80]. At substantially higher temperatures of coal burning for industrial purposes, barite decomposes into BaO, which, in turn, may react with airborne sulphuric acid to produce nanometre-sized secondary barite.

Geogenic grains of silicates and aluminosilicates, which are resistant to weathering, may be related to the composition of the castle's stones and bricks, the cement and mortar binding the stone blocks, and the local geological background (pieces blown from the ground by the wind). On the other hand, quartz and feldspars belong to the main crystalline components identified in ashes from coal combustion [61].

The particles discussed above are embedded among gypsum crystals, forming a kind of network. In cases of dolomitic limestone, dolomite blocks, and bricks, gypsum is occasionally accompanied by hydrated magnesium sulphates—hexahydrite and/or pentahydrate. These secondary sulphate minerals could have primarily formed in the reaction between rock or building material components, mainly calcite $CaCO_3$, and dolomite $CaMg(CO_3)_2$, and polluted atmosphere (presence of sulphur oxides; wet and dry deposition) [2,55]. The presence of magnesium sulphates of various hydration states may suggest that hydration/dehydration processes are taking place, which may result in stone damage due to the crystallisation pressure generated during these processes [45,81,82]. The formation of gypsum ($CaSO_4 \cdot 2H_2O$), the main component of black crusts, also exerts mechanical stress on stones due to its significantly higher molecular volume compared to calcite ($CaCO_3$).

The crystallisation of calcium sulphate dihydrate and the presence of carbonaceous particles are two important factors in the formation of black crust. The metallic compounds of the particulate matter in polluted environments and higher concentrations of carbonaceous particles enhance the SO_4^{2-} formation on stone surfaces [21]. Metals such as Mn, Fe, Zn, Cu, and Ti are efficient catalysts for the oxidation of SO_2 into SO_4^{2-} [35]. Another crucial factor that significantly increases the reaction rate of sulphate formation is the concentration of NO_x in polluted air, with NO_2 acting as an oxidant. Nitrates, occasionally observed in the crust, may be related to the transformation of substrate minerals containing potassium (e.g., feldspars present in mortars, plaster, bricks, and stones) specifically in the presence of nitrogen oxides in a polluted atmosphere. The principal sources of nitrogen oxides in the air are emissions from vehicle exhaust and industry. In recent years, increasing concentrations of nitrates among the crust constituents and in the form of efflorescences and subflorescences appearing on historic monuments in Krakow have been reported [28,55]. On the other hand, NO_x gases can be oxidised by lithotrophic bacteria into nitric acid,

which also contributes to stone decay [26,27]. Nitrate formation on stone surfaces may also be related to animal activity. Bird droppings are a potential source of a wide range of soluble salts and uric acid, generating, among others, phosphates and/or nitrates on the surface [24,57,82].

The existence of microorganisms in the crust covering the blocks is confirmed by the presence of carotenoids. The β-carotene recorded indicates that the carotenoid-producing alga *Trentepohlia* was present at the sampled sites. As this component has only been occasionally recorded, and no macroscopically visible discolouration was observed on the stone surface, the presence of *Trentepohlia* is rather sporadic. Other organic compounds, such as products of microbial metabolism and their reactions with substrates (e.g., oxalates—whewellite and weddellite, characteristic of fungal presence) were not detected [30]. However, a deeper investigation of microbiological activity on the stone surface is beyond the scope of this research.

Finally, the calcium carbonate recorded occasionally on the black surface of bricks is most likely related to the dissolution and leaching of lime-sand or cement-lime mortars binding the structural blocks and the karstification of the adjacent limestone blocks. It should be noted that calcite may also be linked to the carbonation process of hydrated calcium oxide $Ca(OH)_2$ present in bricks [83]. In a polluted atmosphere, calcium carbonate present on the brick surface may become a substrate in a reaction to form hydrated calcium sulphate, i.e., gypsum.

The results demonstrate that degradation symptoms, such as black crust, are closely related to pollution not only in big cities and other urban environments but also in rural areas affected by surrounding industrial and urban complexes. This implies that the protection of heritage buildings in rural areas is also an urgent task. The study confirms that the crust composition could be considered an important natural sensor of air pollution in rural areas. These facts should aid stone conservators in planning the most appropriate strategies for protecting monuments and preventing the deposition of contaminants on the surface, using various conservation cleaning methods.

6. Conclusions

The study aimed to analyse the composition and determine the nature of the black crust and soiling formed on the historic stones and bricks of Lipowiec Castle (southern Poland), located in the countryside. To the authors' knowledge, this is the first study of its kind for this castle as well as for a rural region. The non-destructive RS and SEM-EDS methods employed facilitated a detailed analysis of the crust components.

The examined black crust, relatively uniform in composition, consists of gypsum with minor admixtures of hydrated magnesium sulphates in some samples. Carbonaceous soot, siliceous fly ash, and spherical metal-bearing particles (containing Fe, Mn, Ti, Zn, Cu, Pb, and Cr) do not form a continuous layer but are dispersed among the sulphate crust components. Irregular and sharp-edge-shaped particles contain significant amounts of metals such as Cr, Fe, Mn, Cu, Zn, Pb, and As. The moderate content of carbonaceous particles may suggest a certain self-cleaning of the castle stones exposed to the actions of wind and rainfall, partly washing away some of the black deposits.

Although the Lipowiec Castle is situated in a rural part of the region, its proximity to large industrial and urban complexes, coupled with prevailing NW winds, exposes it to harmful pollutants from the neighbouring industrial and urban centres. The composition of the analysed particles reflects the state of air pollution in the region.

This confirms that ongoing studies on soiling and black crust covering architectural heritage objects can be used as an environmental indicator of the state and trends of air pollution. Such studies should also yield data on past pollution levels.

Black crust and soiling monitoring may be one of the preventive conservation measures, providing data for analyses of the impact of air pollution on the deterioration of heritage buildings over time. This, in turn, should facilitate the adoption of preventive

countermeasures to reduce risks associated with potential environmental pollution and ensure the long-term preservation of the architectural heritage.

Author Contributions: Conceptualisation and methodology, M.M.; software, validation and formal analysis, M.M. and A.G.; investigation M.M., A.G. and K.D.; writing—original draft preparation, M.M. and K.D.; writing—review and editing, M.M. and K.D.; visualisation, M.M. and A.G.; supervision and project administration, M.M.; funding acquisition, M.M. and A.G. All authors have read and agreed to the published version of the manuscript.

Funding: The studies were supported by the AGH University of Krakow, grant number 16.16.140.315.

Institutional Review Board Statement: Not applicable.

Informed Consent Statement: Not applicable.

Data Availability Statement: Data are contained within the article.

Acknowledgments: The authors acknowledge the help of Karolina Pachuta from the Conservation and Renovation Company Piotr Białko Ltd., Kraków, Poland in sampling the historic monument. The authors thank three anonymous reviewers for their comments, which allowed us to improve the manuscript.

Conflicts of Interest: The authors declare no conflicts of interest.

References

1. Doehne, E.; Price, C.A. *Stone Conservations: An Overview of Current Research*, 2nd ed.; Getty Conservation Institute: Los Angeles, CA, USA, 2010; 159p.
2. Lefèvre, R.A.; Ausset, P. Atmospheric pollution and building materials: Stone and glass. In *Natural Stone, Weathering Phenomena, Conservation Strategies and Case Studies*; Siegesmund, S., Weiss, T., Vollbrecht, A., Eds.; Geological Society: London, UK; Special Publications: London, UK, 2002; Volume 205, pp. 329–345. [CrossRef]
3. Saiz-Jimenez, C.; Hermosin, B. Black crusts in the European built environment. *Corros. Rev.* **2004**, *22*, 381–393. [CrossRef]
4. Toniolo, L.; Zerbi, C.M.; Bugini, R. Black layers on historical architecture. *Environ. Sci. Pollut. Res.* **2009**, *16*, 218–226. [CrossRef] [PubMed]
5. Bonazza, A.; Sabbioni, C.; Ghedini, N. Quantitative data on carbon fractions in interpretation of black crusts and soiling on European built heritage. *Atmos. Environ.* **2005**, *39*, 2607–2618. [CrossRef]
6. Grossi, C.M.; Brimblecombe, P. Effect of Long-Term Changes in Air Pollution and Climate on the Decay and Blackening of European Stone Buildings. In *Building Stone Decay: From Diagnosis to Conservation*; Prikryl, R., Smith, B.J., Eds.; Geological Society: London, UK; Special Publications: London, UK, 2007; Volume 271, pp. 117–130. [CrossRef]
7. Fronteau, G.; Schneider-Thomachot, C.; Chopin, E.; Barbin, V.; Mouze, D.; Pascal, A. Black-Crust Growth and Interaction with Underlying Limestone Microfacies. In *Natural Stone Resources for Historical Monuments*; Prikryl, R., Smith, B.J., Eds.; Geological Society: London, UK; Special Publications: London, UK, 2010; Volume 333, pp. 25–34. [CrossRef]
8. Perez-Monserrat, E.M.; Varas-Muriel, M.J.; De Buergo, M.A.; Fort, R. Black Layers of Decay and Color Patterns on Heritage Limestone as Markers of Environmental Change. *Geosciences* **2016**, *6*, 4. [CrossRef]
9. Cano, H.; Ríos-Rojas, J.F.; Hernández-Fernández, J.; Bernal Herrera, W.; Bautista Betancur, M.; De La Hoz Vélez, L.; Agámez González, L. Impact of Environmental Pollution in the Sustainability of Architectural Heritage: Case Study from Cartagena of India, Colombia. *Sustainability* **2022**, *14*, 189. [CrossRef]
10. Brimblecombe, P.; Grossi, C.M. Aesthetic thresholds and blackening of stone buildings. *Sci. Total Environ.* **2005**, *349*, 175–189. [CrossRef] [PubMed]
11. Schiavon, N.; Chiavari, G.; Fabbri, D. Soiling of limestone in an urban environment characterized by heavy vehicular exhaust emissions. *Environ. Geol.* **2004**, *46*, 448–455. [CrossRef]
12. Charola, A.; Pühringer, J.; Steiger, M. Gypsum: A review of its role in the deterioration of building materials. *Environ. Geol.* **2007**, *52*, 339–352. [CrossRef]
13. Barca, D.; Belfiore, C.M.; Crisci, G.M.; La Russa, M.F.; Pezzino, A.; Ruffolo, S.A. Application of laser ablation ICP-MS and traditional techniques to the study of black crusts on building stones: A new methodological approach. *Environ. Sci. Poll. Res.* **2010**, *17*, 1433–1447. [CrossRef]
14. Barca, D.; Comite, V.; Belfiore, C.M.; Bonazza, A.; La Russa, M.F.; Ruffolo, S.A.; Crisci, G.M.; Pezzino, A.; Sabbioni, C. Impact of air pollution in deterioration of carbonate building materials in Italian urban environments. *Appl. Geochem.* **2014**, *48*, 122–131. [CrossRef]
15. Ruffolo, S.A.; Comite, V.; La Russa, M.F.; Belfiore, C.M.; Barca, D.; Bonazza, A.; Crisci, G.M.; Pezzino, A.; Sabbioni, C. An analysis of the black crusts from the Seville Cathedral: A challenge to deepen the understanding of the relationships among microstructure, microchemical features and pollution sources. *Sci. Tot. Environ.* **2015**, *502*, 157–166. [CrossRef] [PubMed]

16. Morillas, H.; Maguregui, M.; García-Florentino, C.; Carrero, J.A.; Madariaga, J.M. The cauliflower-like black crusts on sandstones: A natural passive sampler to evaluate the surrounding environmental pollution. *Environ. Res.* **2016**, *17*, 218–232. [CrossRef] [PubMed]
17. Calparsoro, E.; Maguregui, M.; Giakoumaki, A.; Morillas, H.; Madariaga, J.M. Evaluation of black crust formation and soiling process on historical buildings from the Bilbao metropolitan area (north of Spain) using SEM-EDS and Raman microscopy. *Environ. Sci. Pollut. Res.* **2017**, *24*, 9468–9480. [CrossRef] [PubMed]
18. Amoroso, G.G.; Fassina, V. *Stone Decay and Conservation. Atmospheric Pollution, Cleaning, Consolidation and Protection*; Elsevier: Amsterdam, The Netherlands, 1983; 449p.
19. Johansson, L.G.; Lindqvist, O.; Mangio, R.E. Corrosion of calcareous stones in humid air containing SO_2 and NO_2. Dur. *Build. Mat.* **1988**, *5*, 439–449.
20. Moropoulou, A.; Bisbikou, K.; Van Grieken, R.; Zezza, F.; Macri, F. Origin and growth of weathering crusts on ancient marbles in industrial atmosphere. *Atmos. Environ.* **1998**, *32*, 967–982. [CrossRef]
21. Charola, A.E.; Ware, R. Acid deposition and the deterioration of stone: A brief review of a broad topic. In *Natural Stone, Weathering Phenomena, Conservation Strategies and Case Studies*; Siegesmund, S., Weiss, T., Vollbrecht, A., Eds.; Geological Society: London, UK; Special Publications: London, UK, 2002; Volume 205, pp. 393–406. [CrossRef]
22. ICOMOS. 2008. Available online: http://www.icomos.org/en/component/content/article/116-englishcategories/resources/publications/261-monumentsasites-xv (accessed on 10 April 2024).
23. La Russa, M.F.; Comite, V.; Aly, N.; Barca, D.; Fermo, P.; Rovella, N.; Antonelli, F.; Tesser, E.; Aquino, M.; Ruffolo, S.A. Black crusts on Venetian built heritage, investigation on the impact of pollution sources on their composition. *Eur. Phys. J. Plus* **2018**, *133*, 370. [CrossRef]
24. Machill, S.; Althaus, K.; Krumbein, W.E.; Stegew, W.E. Identification of organic compounds extracted from black weathered surfaces of Saxonean sandstones, correlation with atmospheric input and rock inhabiting microflora. *Org. Geochem.* **1997**, *27*, 79–97. [CrossRef]
25. Sýkorová, I.; Havelcová, M.; Zeman, A.; Trejtnarová, H. Carbon air pollution reflected in deposits on chosen building materials of Prague Castle. *Sci. Total Environ.* **2011**, *409*, 4606–4611. [CrossRef] [PubMed]
26. Papida, S.; Marphy, W.; May, E. Enhancement of physical weathering of building stones by microbial populations. *Int. Biodeter. Biodegr.* **2000**, *46*, 305–317. [CrossRef]
27. De Belie, N. Microorganisms versus stony materials: A love–hate relationship. *Mat. Struct.* **2010**, *43*, 1191–1202. [CrossRef]
28. Marszałek, M.; Dudek, K.; Czerny, J.; Gaweł, A. Mineralogical and geochemical studies of secondary mineral assemblages related to deterioration of building materials. *Geol. Quart.* **2019**, *63*, 683–698. [CrossRef]
29. Marszałek, M.; Dudek, K.; Gaweł, A. Cement Render and Mortar and Their Damages Due to Salt Crystallization in the Holy Trinity Church, Dominicans Monastery in Cracow, Poland. *Minerals* **2020**, *10*, 641. [CrossRef]
30. Gaylarde, C.C.; Baptista-Neto, J.A. Microbiologically induced aesthetic and structural changes to dimension stone. *npj Mater. Degrad.* **2021**, *5*, 33. [CrossRef]
31. Pozo-Antonio, J.S.; Cardell, C.; Comite, V.; Fermo, P. Characterization of black crusts developed on historic stones with diverse mineralogy under different air quality environments. *Environ. Sci. Pollut. Res.* **2022**, *29*, 29438–29454. [CrossRef] [PubMed]
32. Islam, N.; Roy, K.; Barman, P.; Rabha, S.; Bora, H.K.; Khare, P.; Konwar, R.; Saikia, B.K. Chemical and toxicological studies on black crust formed over historical monuments as a probable health hazard. *J. Hazard. Mat.* **2024**, *464*, 132939. [CrossRef] [PubMed]
33. Török, Á.; Licha, T.; Simon, K.; Siegesmund, S. Urban and rural limestone weathering; the contribution of dust to black crust formation. *Environ. Earth. Sci.* **2011**, *63*, 675–693. [CrossRef]
34. Randazzo, L.; Collina, M.; Ricca, M.; Barbieri, L.; Bruno, F.; Arcudi, A.; La Russa, M.F. Damage Indices and Photogrammetry for Decay Assessment of Stone-Built Cultural Heritage: The Case Study of the San Domenico Church Main Entrance Portal (South Calabria, Italy). *Sustainability* **2020**, *12*, 5198. [CrossRef]
35. Camuffo, D.; Del Monte, M.; Sabbioni, C. Origin and growth mechanisms of the sulfated crusts on urban limestone. *Water Air Soil Poll.* **1983**, *19*, 351–359. [CrossRef]
36. Małkowska-Holcerowa, T. *Lipowiec dawny zamek biskupów krakowskich. (Lipowiec the Former Castle of Cracow's Bishops)*; Wyd. PTTK "KRAJ": Warszawa, Poland, 1989; 44p. (In Polish with English Summary)
37. Siedlecki, S. Utwory geologiczne obszaru pomiędzy Chrzanowem a Kwaczałą. (Geology of the area between Chrzanów and Kwaczała). *Biul. Inst. Geol.* **1952**, *60*, 1–230. (In Polish with English Summary)
38. Płonczyński, J.; Preidl, M.; Kurek, S. *Objaśnienia do szczegółowej mapy geologicznej Polski 1:50 000 Arkusz Chrzanów (971). (Explanations to Detailed Geological Map of Poland 1:50000 Sheet Chrzanów (971))*; Państwowy Instytut Geologiczny—Państwowy Instytut Badawczy: Warszawa, Poland, 2015; 41p. (In Polish)
39. Myszkowska, J. Litofacje i sedymentacja dolomitów diploporowych (środkowy wapień muszlowy) wschodniej części obszaru śląsko-krakowskiego. (Lithofacies and Sedimentation of Diplopora Dolomite (Middle Muschelkalk) in the East Part of the Cracovian-Silesian Region). *Ann. Soc. Geol. Pol.* **1992**, *62*, 19–62. (In Polish with English Summary)
40. Wyszomirski, P.; Przytuła, S. Charakterystyka surowcowa kruszywa dolomitowego na przykładzie kopaliny z Libiąża (region śląsko-krakowski). (Raw mineral characteristics of dolostone aggregates: An example of the rock from Libiąż (Cracow-Silesian region)). *Zesz. Nauk. IGSMiE PAN* **2010**, *79*, 213–222. (In Polish with English Abstract)

41. Downs, R.T.; Hall-Wallace, M. A Database of Crystal Structures. Published in the American Mineralogist and The Canadian Mineralogist and Its Use as a Resource in the Classroom. In Proceedings of the 18th General Meeting of the International Mineralogical Association, Edinburgh, UK, 1–6 September 2002; p. 128.
42. Wang, A.; Freeman, J.J.; Jolliff, B.L.; Chou, I. Sulfates on Mars: A systematic Raman spectroscopic study of hydration states of magnesium sulfates. *Geochim. Cosmochim. Acta* **2006**, *70*, 6118–6135. [CrossRef]
43. Culka, A.; Košek, F.; Drahota, P.; Jehlička, J. Use of miniaturized Raman spectrometer for detection of sulfates of different hydration states—Significance for Mars studies. *Icarus* **2014**, *243*, 440–453. [CrossRef]
44. Jehlička, J.; Culka, A.; Košek, F. Obtaining Raman spectra of minerals and carbonaceous matter using a portable sequentially shifted excitation Raman spectrometer—A few examples. *J. Raman Spectr.* **2017**, *48*, 1583–1589. [CrossRef]
45. Steiger, M.; Linnow, K.; Juling, H.; Gülker, G.; Jarad, A.; Brüggerhoff, S.; Kirchner, D. Hydration of $MgSO_4 \cdot H_2O$ and Generation of Stress in Porous Materials. *Cryst. Growth Des.* **2008**, *8*, 336–343. [CrossRef]
46. Mernag, T.P.; Cooney, R.P.; Johnson, R.A. Raman Spectra of Graphon Carbon Black. *Carbon* **1984**, *22*, 39–42. [CrossRef]
47. Lee, K.O.; Cole, R.; Sekar, R.; Choi, M.Y.; Kang, J.S.; Bae, C.S.; Shin, H.D. Morphological Investigation of the Microstructure, Dimensions, and Fractal Geometry of Diesel Particulates. *Proc. Combust. Inst.* **2002**, *29*, 647–653. [CrossRef]
48. Soewono, A.; Rogak, S. Morphology and Raman Spectra of Engine-Emitted Particulates. *Aerosol Sci. Technol.* **2011**, *45*, 1206–1216. [CrossRef]
49. Sadezky, A.; Muckenhuber, H.; Grothe, H.; Niessner, R.; Pöschl, U. Raman Spectra of Soot and Related Carbonaceous Materials: Spectral Analysis and Structural Information. *Carbon* **2005**, *43*, 1731–1742. [CrossRef]
50. Schito, A.; Romano, C.; Corrado, S.; Grido, D.; Poe, B. Diagenetic thermal evolution of organic matter by Raman spectroscopy. *Org. Geochem.* **2017**, *106*, 57–67. [CrossRef]
51. Henry, D.G.; Jarvis, I.; Gillmore, G.; Stephenson, M. Raman spectroscopy as a tool to determine the thermal maturity of organic matter: Application to sedimentary, metamorphic and structural geology. *Earth-Sci. Rev.* **2019**, *198*, 102936. [CrossRef]
52. Chhowalla, M.; Ferrari, A.C.; Robertson, J.; Amaratunga, G.A. Evolution of sp2 Bonding with Deposition Temperature in Tetrahedral Amorphous Carbon Studied by Raman Spectroscopy. *Appl. Phys. Lett.* **2000**, *76*, 1419–1421. [CrossRef]
53. Ferrari, A.C.; Robertson, J. Interpretation of Raman Spectra of Disordered and Amorphous Carbon. *Phys. Rev. B* **2000**, *61*, 14095–14107. [CrossRef]
54. Tuinstra, F.; Koenig, J.L. Raman Spectrum of Graphite. *Chem. Phys.* **1970**, *53*, 1126–1130. [CrossRef]
55. Marszałek, M. Identification of secondary salts and their sources in deteriorated stone monuments using micro-Raman spectroscopy, SEM-EDS and XRD. *J. Raman Spectr.* **2016**, *47*, 1473–1485. [CrossRef]
56. Adar, F. Carotenoids—Their Resonance Raman Spectra and How They Can Be Helpful in Characterizing a Number of Biological Systems. *Spectroscopy* **2017**, *32*, 12–20. Available online: https://www.spectroscopyonline.com/authors/fran-adar (accessed on 23 February 2024).
57. Kloppmann, W.; Bromblet, P.; Vallet, J.M.; Vergès-Belmin, V.; Rolland, O.; Guerrot, C.; Gosselin, C. Building materials as intrinsic sources of sulphate: A hidden face of salt weathering of historical monuments investigated through multi-isotope tracing (B, O, S). Sci. *Total Env.* **2011**, *409*, 1658–1669. [CrossRef]
58. Ishihara, J.; Takahashi, H. Raman spectral analysis of microbial pigment compositions in vegetative cells and heterocysts of multicellular cyanobacterium. *Biochem. Biophys. Rep.* **2023**, *34*, 101469. [CrossRef] [PubMed]
59. Pietras, B.G. The Origin of Dust Particles in Atmospheric Air in Krakow (Poland) (Atmospheric Background). *Land* **2022**, *11*, 155. [CrossRef]
60. Zioła, N.; Banasik, K.; Jabłońska, M.; Janeczek, J.; Błaszczak, B.; Klejnowski, K.; Mathews, B. Seasonality of the airborne ambient soot predominant emission sources determined by Raman microspectroscopy and thermo-optical method. *Atmosphere* **2021**, *12*, 768. [CrossRef]
61. Smołka-Danielowska, D. Trace elements and mineral composition of waste produced in the process of combustion of solid fuels in individual household furnaces in the Upper Silesian Industrial Region (Poland). *Environ. Socio-Econ. Stud.* **2015**, *3*, 30–38. [CrossRef]
62. Smolka-Danielowska, D.; Fiedor, D. Potentially toxic elements in fly ash dependently of applied technology of hard coal combustion. *Environ. Sci. Pollut. Res.* **2018**, *25*, 25091–25097. [CrossRef] [PubMed]
63. Sass-Gustkiewicz, M. Revised and completed paragenetic order of minerals in the Pomorzany lead-zinc deposit. Upper Silesian Region, Poland. *Mineral. Pol.* **1997**, *28*, 46–80.
64. Mikulski, S.Z.; Oszczepalski, S.; Sadłowska, K.; Chmielewski, A.; Małek, R. Występowanie pierwiastków towarzyszących i krytycznych w wybranych udokumentowanych złożach rud Zn-Pb, Cu-Ag, Fe-Ti-V, Mo-Cu-W, Sn, Au-Asi Ni w Polsce. (The occurrence of associated and critical elements in the selected documented Zn-Pb, Cu-Ag, Fe-Ti-V, Mo-Cu-W, Sn, Au-As and Ni deposits in Poland). *Biul. Państwowego Inst. Geol.* **2018**, *472*, 21–52. (In Polish with English Abstract) [CrossRef]
65. Cabała, J. *Metale ciężkie w środowisku glebowym olkuskiego rejonu eksploatacji rud Zn-Pb. (Heavy Metals in Ground Soil Environment of the Olkusz Area of Zn-Pb Ore Exploitation)*; Silesia Univeristy Press: Katowice, Poland, 2009; 130p. (In Polish with English Summary). Available online: http://hdl.handle.net/20.500.12128/3415 (accessed on 23 February 2024).
66. Anameric, B.; Komar Kawatra, S. Direct iron smelting reduction processes Mineral Processing and Extractive Metallurgy Review. *Int. J.* **2008**, *30*, 1–51. [CrossRef]

67. Jabłońska, M.; Rachwał, M.; Wawer, M.; Kądziołka-Gaweł, M.; Teper, E.; Krzykawski, T.; Smołka-Danielowska, D. Mineralogical and chemical specificity of dusts originating from iron and non-ferrous metallurgy in the light of their magnetic susceptibility. *Minerals* **2021**, *11*, 216. [CrossRef]
68. Marszałek, M. Application of optical microscopy and scanning electron microscopy to the study of stone weathering: A Cracow case study. *Int. J. Archit. Herit.* **2008**, *2*, 83–92. [CrossRef]
69. Del Monte, M.; Nanni, T.; Tagliazucca, M. The origin of black magnetic spherules through a study of their chemical, physical and mineralogical characteristics. *Annali di Geofis.* **1976**, *29*, 9–25. [CrossRef]
70. Ramsden, A.R.; Shibaoka, M. Characterization and analysis of individual fly-ash particles from coal-fired power stations by a combination microscopy and quantitative electron microprobe analysis. *Atmos. Environ.* **1982**, *16*, 2191–2206. [CrossRef]
71. Rożek, D.; Nadłonek, W.; Cabała, J. Forms of heavy metals (Zn, Pb, Cd) occurring in rhizospheres from the areas of former and contemporary Zn-Pb ore mining. *Min. Sci.* **2015**, *22*, 125–138. [CrossRef]
72. Kicińska, A.; Gruszecka-Kosowska, A. Long-term changes of metal contents in two metallophyte species (Olkusz area of Zn-Pb ores, Poland). *Environ. Monit. Assess.* **2016**, *188*, 339. [CrossRef] [PubMed]
73. Pope, C.A.; Ezzati, M.; Dockery, D.W. Fine-particulate air pollution and life expectancy in the United States. *N. Engl. J. Med.* **2009**, *360*, 376–386. [CrossRef]
74. Brunekreef, B.; Forsberg, B. Epidemiological evidence of effects of coarse airborne particles on health. *Eur. Respir. J.* **2005**, *26*, 309–318. [CrossRef] [PubMed]
75. Mills, A.; Le Hunte, S. An Overview of Semiconductor Photocatalysis. *J. Photochem. Photobiol. A Chem.* **1997**, *108*, 1–35. [CrossRef]
76. Wang, D.; Leng, Z.; Yu, H.; Hüben, M.; Kollmann, J.; Oese, M. Durability of epoxy-bonded TiO_2-modified aggregate as a photocatalytic coating layer form asphalt pavement under vehicle tire polishing. *Wear* **2017**, *382–383*, 1–7. [CrossRef]
77. Morillas, H.; Marcaida, I.; Maguregui, M.; Upasen, S.; Gallego-Cartagena, E.; Madariaga, J.M. Identification of metals and metalloids as hazardous elements in $PM_{2.5}$ and PM_{10} collected in a coastal environment affected by diffuse contamination. *J. Clean. Prod.* **2019**, *226*, 369–378. [CrossRef]
78. Boggs, S., Jr. *Petrology of Sedimentary Rocks*, 2nd ed.; Cambridge University Press: London, UK, 2009; 600p. [CrossRef]
79. Stanienda, K. Fazy mineralne w skałach węglanowych warstw gogolińskich obszaru Śląska Opolskiego. (Mineral Phases in Carbonate Rocks of the Gogolin Beds from the Area of Opole Silesia). *Gospod. Surowcami Miner.–Miner. Resour. Manag.* **2014**, *30*, 17–42. (In Polish with English Abstract) [CrossRef]
80. Jabłońska, M.; Rietmeijer, F.J.M.; Janeczek, J. Fine-grained barite in coal fly ash from the Upper Silesian industrial region. *Environ. Geol.* **2001**, *40*, 941–948. [CrossRef]
81. Gázquez, F.; Rull, F.; Medina, J.; Sanz-Arranz, A.; Sanz, C. Linking groundwater pollution to the decay of 15th-century sculptures in Burgos Cathedral (northern Spain). *Environ. Sci. Pollut. Res.* **2015**, *22*, 15677–15689. [CrossRef]
82. Benavente, D.; de Jongh, M.; Cañaveras, J.C. Weathering Processes and Mechanisms Caused by Capillary Waters and Pigeon Droppings on Porous Limestones. *Minerals* **2021**, *11*, 18. [CrossRef]
83. Coletti, C.; Cesareo, L.P.; Nava, J.; Germinario, L.; Maritan, L.; Massironi, M.; Mazzoli, C. Deterioration Effects on Bricks Masonry in the Venice Lagoon Cultural Heritage: Study of the Main Façade of the Santa Maria dei Servi Church (14th Century). *Heritage* **2023**, *6*, 1277–1292. [CrossRef]